ON RIEMANNIAN GEOMETRIES OF VISUAL SPACE

Jacek Turski*
Department of Mathematics and Statistics
University of Houston-Downtown
Houston, TX 77002
turskij@gmail.com

June 2, 2022

ABSTRACT

This is a study of the phenomenal geometries constructed in the Riemannian geometry framework from simulated iso-disparity conics in the horizontal visual plane of the binocular system with the asymmetric eyes (AEs). For the eyes' resting vergence posture, which depends on parameters of the AE, the iso-disparity conics are frontal straight lines in physical space. For all other fixations, the iso-disparity conics consist of families of the ellipses or hyperbolas depending on both the AE's parameters and the bifoveal fixation. However, the iso-disparity conic's arcs in the gaze direction are perceived as the frontal lines and are referred to as geodesics in visual space. Thus, geometries of physical and visual spaces are different. An assumption underlying the relevant architecture of the human visual system is combined with results from simulated iso-disparity straight lines, giving the relative depth as a function of the distance. This establishes the metric tensor in binocular space of fixations for the eyes' resting vergence posture. The resulting geodesics in the gaze direction, give the distance to the horizon and zero curvature. For all other fixations, only the sign of the curvature can be inferred from the global behavior of the simulated iso-disparity conics.

***K*eywords** Binocular correspondence, asymmetric model eye, iso-disparity conics, visual space, Riemannian geometry, metric tensor, geodesics, curvature

1 Introduction

Though the study of phenomenal visual space has had a long history, the geometric relationship between phenomenal visual space and the stimuli-containing physical space remains unresolved. The main reason is that the spatial relations of phenomenal space such as depth and size are, in general, task-dependent and influenced by both contextual factors and our expectations. However, the binocular disparity provides the most precise depth cue that is sufficient for stereopsis with no explicit recognition of form such that the resulting perception is generally unaffected by other factors.

Here, I investigate the disparity-based phenomenal geometry in the binocular system with the asymmetric eyes (AEs) in the framework of the bicentric perspective projections [22]. The AE model is comprised of the fovea's displacement from the posterior pole by angle $\alpha = 5.2°$ and the crystalline lens' tilt by angle β. Angle alpha is relatively stable in the human population and angle β varies between $-0.4°$ and $4.7°$ [21]. In the human eye, the fovea's displacement from the posterior pole and the cornea's asphericity contribute to optical aberrations that the lens' tilt then partially compensates for [1].

The horopteric conics simulated in [22] resemble the empirical horopters and are extended in this study to the families of iso-disparity conics. These iso-disparity curves are perceived as the frontal straight lines and are referred to as visual geodesics.

For the eyes in the resting vergence posture, that is, when eyes fixate at the abathic distance, the iso-disparity curves are straight frontal lines in physical space. For other fixations, the iso-disparity curves consist of either a family of ellipses

*Professor Emeritus

or hyperbolas, depending on the location of the fixation point. Because the iso-disparity curves are always perceived as frontal lines in the binocular field, the geometries of physical space and phenomenal visual space are different and unraveling this difference global aspects is the main goal of this work

2 Binocular correspondence

The correspondence of retinal elements is not readily available in nonius measurements of longitudinal horopter [23]. It is not available also from geometrical methods because of the eye's asymmetry: the corresponding points are compressed in the temporal retinae relative to those in the nasal retinae [19]. In the theory of binocular system with AE model [22], the natural asymmetry of eye's optical components is represented in the AE by the fovea's displacement from the posterior pole by $\alpha = 5.2°$ and the lens' tilt by β that varies between $-0.4°$ and $4.7°$. The AEs are shown in Figure 1.

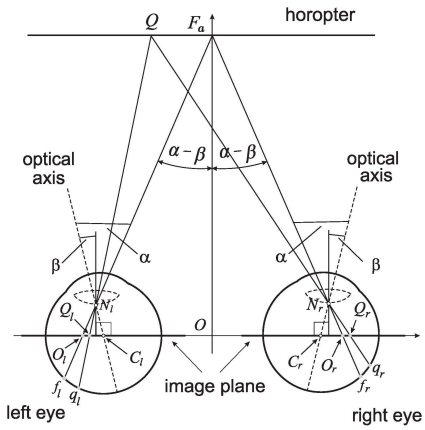

Figure 1: Binocular correspondence. The linear horopter passing through the fixation F_a at the abathic distance $d_a = |OF_a|$. The fixation point F_a projects to the foveae f_r and f_l and the point Q on the horopter projects to the retinal corresponding points q_r and q_l and to points Q_r and Q_l in the image plane. The subtense σ_a at F_a is given by $2(\alpha - \beta)$ [22].

The distribution of the retinal corresponding points q_r, q_l is asymmetrical with respect to the foveae f_r and and f_l such that $|q_r f_r| \neq |q_l f_l|$, see Figure 1. It is demonstrated in [22], that the distribution of these corresponding points projected into the image planes of each AE, Q_r, Q_l, satisfy $|Q_r O_r| = |Q_l O_l|$ where O_r and O_l are projected foveae f_r and f_l, respectively. It is proved in [22] that this symmetry on the image plane is preserved for all other fixations. Thus, unknown (asymmetric) retinal correspondence can be entirely formulated on the image plane of the AE in terms of the asymmetry parameters.

The distance $d_a = |OF_a|$ to the fixation point F_a in the posture with coplanar image planes is distinguished by linear horopter shown in Figure 1 and is known as the abathic distance. It was obtained in [22] as follows:

$$d_a = \frac{a\cos(\alpha - \beta) + 0.6\sin\alpha}{\sin(\alpha - \beta)}, \tag{1}$$

where $2a = 6.5$ cm is the ocular separation and 0.6 cm is the distance of the nodal point from the eyeball's rotation center.

The image plane in the AE model is parallel to the lens's equatorial plane and is passing through the eye's rotation center. Figure 1 shows the eyes' posture in which the image planes are coplanar and the horopter is frontal straight line passing through the fixation point at the abathic distance. This fixation is resulting in the eyes resting vergence posture [12]. Because the eye muscles' natural tonus resting position serves as a zero-reference level for convergence effort [7], this eye posture is identified in [22] with the eyes' primary (binocular) position.

3 Binocular Field of Fixations

For an observer with a stationary, upright head and binocular fixations in the horizontal plane, the coordinate system consists of the y-axis passing through the eyes' rotation centers and the head z-axis formed by the intersection of the

midsagittal plane with the horizontal visual plane. The binocular field of fixations is limited by the head/eyes anatomy and physiology. In fact, this set is limited by the protruded nose and the fixations neurally restricted to the azimuthal range $\pm 45°$ [9].

Further, the geometry of the eyes in symmetric convergence shown in Figure 1, demonstrate that the binocular system possesses bilateral symmetry—the symmetry with respect to the head's midsagittal plane. Therefore, the binocular field of fixation, denoted by B, is assumed symmetric about the z-axis. Thus, B is a convex set shown in Figure 2 where the point $(0, z_0)$ denotes the closest point on which the eyes can converge.

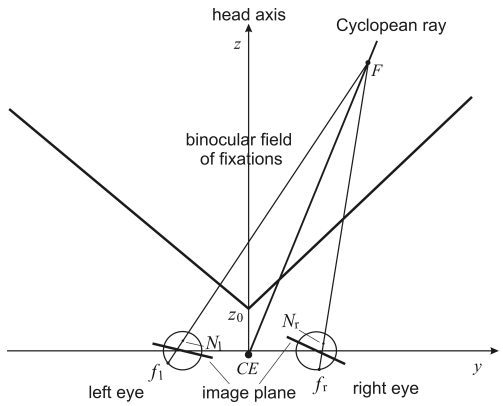

Figure 2: The binocular field of fixations in the horizontal visual plane for the binocular system with the AEs.

For a fixation point, the local chart is the whole set B. For every fixation $(y, z) \in B$, I want to find the corresponding scalar product on the tangent plane, R^2, with its origin at (y, z) using the biologically motivated geometric theory of human binocular perception developed in [22]. These families of scalar products will define the geometries of visual space, each dependent on both the AEs parameters and the point of binocular fixation.

4 Simulation of Iso-Disparity Curves

The simulation of the horopteric conics in [22] is extended here to the iso-disparity curves. The simulations of the iso-disparity conics of a constant disparity difference that are carried out in *GeoGebra* are shown in Figure 3, Figure 4 and in Figure 5 for the same disparity value and different fixations.

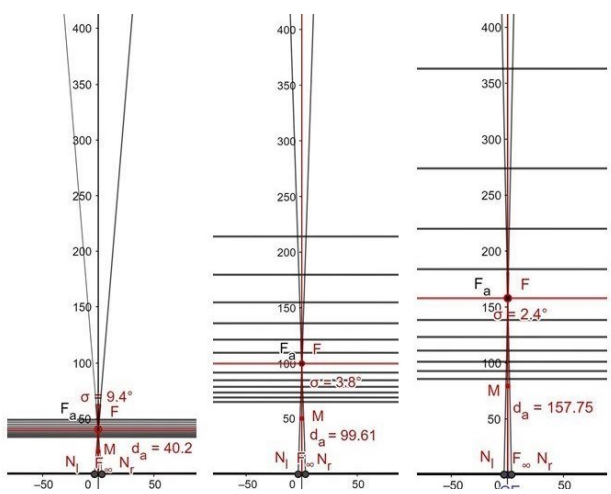

Figure 3: The iso-disparity lines for the eyes' resting vergence fixations with the fixation distance as a function of β given in (1): on the left, the abathic distance $d_a = 40.2$ cm for $\beta = 0.5°$, in the middle, the abathic distance $d_a = 99.61$ cm for $\beta = 3.3°$, and on the left, the abathic distance $d_a = 157,75$ cm for $\beta = 4°$ The horopters are shown in horizontal red lines. The angles at F are $\sigma = 2(\alpha - \beta)$, where $\alpha = 5.2°$.

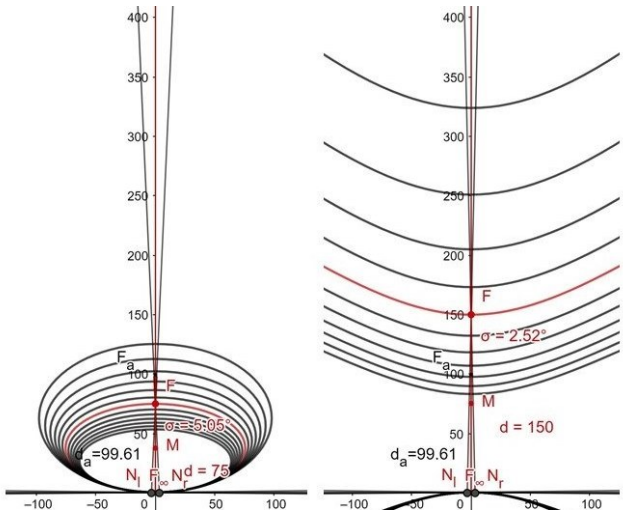

Figure 4: The iso-disparity conics for the binocular system of the abathic distance $d_a = 99.61$ cm for two symmetric fixations at the indicated distances d: ellipses on the left and hyperbolas on the right. The conics in red lines are horopters.

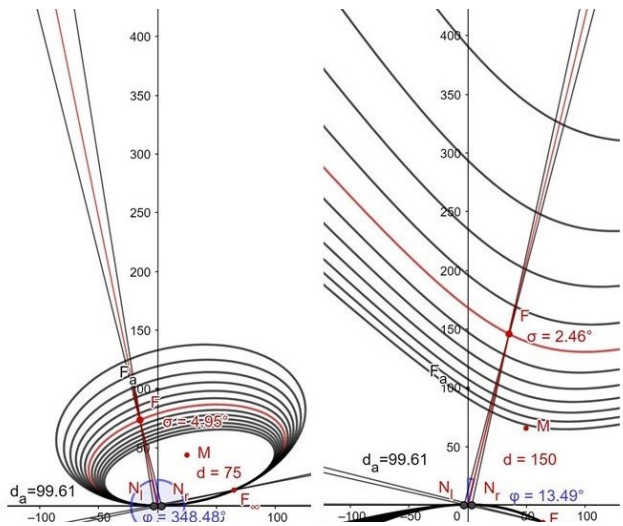

Figure 5: The iso-disparity conics for two asymmetric fixations: ellipses on the left and hyperbolas on the right. The conics in red lines are horopters. The straight line passing through the fixation F is the Cyclopean ray. Its direction specifies the orientation of the conics. The indicated distances d are measured along the Cyclopean ray.

Figure 4 and Figure 5 show how the iso-disparity lines shown in the middle in Figure 3 for $d_a = 99.61$ cm are transformed into ellipses and hyperbolas for symmetric (Figure 4) and asymmetrically (Figure 5) fixated points in the binocular field. All fixation points are of the distance 75 cm and 150 cm along the Cyclopean ray for the ellipses and hyperbolas, respectively. The direction of the Cyclopean ray specifies the orientation of the horopteric conics [22] and, therefore, the orientations of the iso-disparity conics for a given fixation.

For the the above shown simulations, I take a disparity value of $\delta_0 = 0.00355$ cm between each neighboring iso-disparity curves.

5 Relative Depth for Resting Eyes

From the simulations shown in Figure 3 for the disparity step of $\delta_0 = 0.00355$ cm, I calculate the distance Δz_i and midpoint z_i between the consecutive iso-disparity lines to approximate how the depth of iso-disparity lines changes

with distance to the head in the gaze's direction. The points $(z_i, \Delta z_i)$ for different abathic distance eyes fixations lie on the graph of a single quadratic function $\Delta z(z, \delta_0) = 0.000892z^2$ in Figure 6.

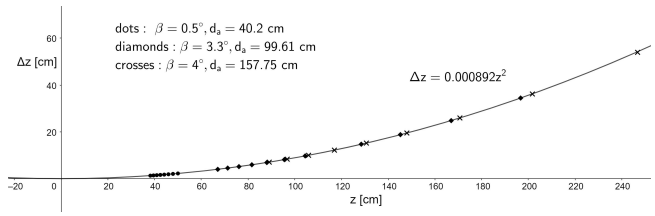

Figure 6: For the simulations shown in Figure 3, the points $(z, \Delta z)$ are plotted for three different abathic distance fixations: $d_a = 40.2$ cm (dots), $d_a = 99.61$ cm (diamonds), and $d_a = 157.75$ cm (crosses).

To investigate the iso-disparity lines distribution dependence on disparity value, I compare simulated iso-disparity lines for disparity difference $\delta_0 = 0.00355$ cm with lines simulated for $\delta = (1/5)\delta_0 = 0.00071$ cm both for the abathic distance $d_a = 99.61$ cm. The result of these two simulations is shown in Figure 7.

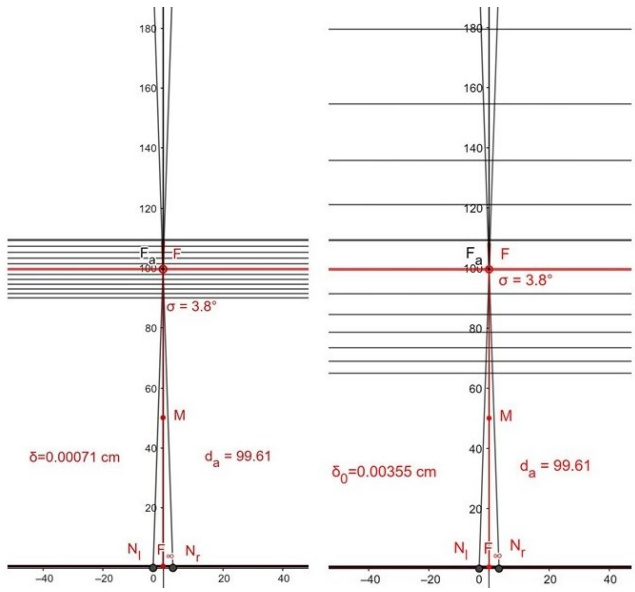

Figure 7: The is-disparity lines for $d_a = 99.61$ cm with different disparity values; on the right, $\delta_0 = 0.00355$ cm, while on the left, $\delta = 0.00071$ cm.

We can see that each space between the neighboring iso-disparity lines for disparity $\delta_0 = 0.00355$ shown in Figure 7's right panel is filled by an additional five iso-disparity lines for disparity $\delta = 0.00071$ shown on the left in Figure 7. Thus, the relation

$$\Delta z(z, \delta) = 0.000178z^2 = \frac{1}{5}0.000892z^2, \tag{2}$$

can be predicted from the simulations and verified numerically. In fact, substituting $d_a = 99.61$ cm for z in (2), we obtain,

$$\begin{aligned} \Delta z(d_a, \delta) &= 0.000178d_a^2 = 1.77 \text{ cm} \\ &= \frac{1}{5}0.000892d_a^2 = \frac{1}{5}8,85 \text{ cm}, \end{aligned} \tag{3}$$

which agree with the simulations shown in Figure 7.

The above discussion of simulations demonstrate that for any $z > 0$, disparity δ, and $h > 0$,

$$\Delta z(z, h\delta) = h\Delta z(z, \delta), \tag{4}$$

This relation can be scaled down to the value of the disparity imposed by the foveal distribution of photoreceptors.

I conclude that the interval between iso-disparity lines for the disparity difference $\delta = h\delta_0$ satisfies the proportionality relation,

$$\Delta z(z, h\delta_0) = h0.000892z^2. \tag{5}$$

I choose the h value such that $\Delta z(d_a, h\delta_0)$ gives the depth resolution at the fovea where the cone-to-cone spacing is about 2.7×10^{-4} cm, which gives the corresponding spacing of 10^{-4} cm on the image plane of the AE. Given that $\delta_0 = 0.00355$ cm, we obtain $h = 10^{-4}/3.55 \times 10^{-3} \approx 1/35$. Thus, for $h = 1/35$,

$$\Delta z(d_a, h\delta_0) = h0.000892d_a^2 = 2.5 \times 10^{-5}d_a^2. \tag{6}$$

To simplify notation, I denote $\Delta z(z, (1/35)\delta_0)$ by $\Delta z(z)$. Then, we obtain from (6): $\Delta z(d_a) \approx 0.25$ cm for $d_a = 99.61$ and $\Delta z(d_a) \approx 0.04$ cm for $d_a = 40.2$.

In order to model relative depth, the simulations must be combined with the fundamental features of the human visual system's architecture, which include the cones' eccentricity dependent density and the convergence of the photoreceptors on the ganglion cells, which is 1-to-1 in the foveala and which approaches 200-to-1 in the periphery. Related to this issue, the concept of receptive fields becomes important. Visual information is sent from the eyes along the ganglion cells' axons and arrives, mainly, at the primary visual cortex, where it is retinotopically mapped with a significant magnification of the foveal region and scaled logarithmically with retinal eccentricity [16]. Because there is no theory based on first principles that can describe how perceived relative depth varies with disparity and distance, I postulate that the relative depth element δp in visual space approximately satisfies the relation.

Postulate. *Postulate The relative depth element δd in visual space is given by*

$$\delta d = \frac{d_a^2}{z^2}\rho(z)\Delta z(z) = \frac{d_a^2}{z^2}\delta z \tag{7}$$

where $\delta z = \Delta z(d_a)$. Here $\rho(z)$ accounts for the anatomical and physiological aspects of the human visual system .

In this work, I want to emphasize the modeling of the global aspects of the visual space geometry that can be studied in the Riemannian geometry framework.

Human disparity contains two components, fine disparity and coarse disparity [17]. Fine disparity allows us to determine the depth of objects in the central visual area where disparate images are fused into a single percept (Panum's fusional area). Coarse disparity provides stereopsis from disparities well beyond the fusible range. It is still useful for depth perception for moderately large disparities even for double images but is only clearly signed with a vague impression of depth magnitude for very large disparity values [3, 25]. Importantly, coarse disparity creates our sense of being immersed in the ambient environment [2].

Some of these global aspects are uncovered by the theory developed here from the perceived relative depth postulated in (7).

6 Metric Tensor for Resting Eyes

In this section, I propose a model of the visual space metric tensor, the fundamental concept of Riemannian geometry. To do this, I first derive the expression for the line element in the y-direction.

The length of projected δy of the iso-disparity line element projected to the Cyclopean eye image is directly proportional to the length of line element δy and inversely proportional to the distance to the iso-disparity line. Assuming the veridical line element perception $\delta\lambda$ at the abathic distance,

$$\delta\lambda(z) = \frac{d_a}{z}\delta y, \tag{8}$$

and combining it with (7), we obtain the visual space metric line element

$$\delta s^2 = \frac{d_a^2}{z^2}\delta y^2 + \frac{d_a^4}{z^4}\delta z^2. \tag{9}$$

The binocular field of fixations B in the horizontal plane was discussed in Section 3. This is a convex set parametrized by the coordinates (y, z) that is shown in Figure 2. The set B has the Cyclopean visual metric determined by a map

$$g : (y, z) \in B \longrightarrow g_{(y,z)} \in M_2, \tag{10}$$

where $g_{(y,z)}$ is the metric tensor obtained from (9),

$$g_{(y,z)} = \begin{pmatrix} \frac{d_a^2}{z^2} & 0 \\ 0 & \frac{d_a^4}{z^4} \end{pmatrix}, \tag{11}$$

and M_2 is the set of all real symmetric positive defined 2×2 matrices.

The visual metric tensor defines an inner product on each tangent plane $T_{(y,z)}B$, the tangent plane R^2 at (y, z) that has the origin at this point. Because $(0, 0) \notin B$, the map g in (10) is a smooth function on B. The inner product is usually written $\langle \partial_y, \partial_z \rangle = g_{(y,z)}(\partial_y, \partial_z)$ for the vector basis $\partial_y, \partial_z \in T_{(y,z)}B$. Thus, the length of the vector V is $||V|| = \sqrt{\langle V, V \rangle}$ and the angle between U and V is $\cos\theta = \langle U, V \rangle / ||U|| ||V||$.

Although I use standard Riemannian geometry notation for writing the basis vectors, it should be understood that for the coordinates (y, z), $\partial_y = (1, 0)$ and $\partial_z = (0, 1)$.

The pair (B, g) is a global chart on the binocular field that allows computing length of vectors in tangent spaces and, therefore, length of curves in B. It emphasizes global aspects of the visual space.

7 Geodesics for Resting Eyes

For an excellent exposition of the Riemannian geometry framework, I refer to [6]. I start by writing the defining expressions for the Christoffel symbols

$$\Gamma^i_{jk} = \sum_l \frac{1}{2} g^{il} (g_{lk,j} + g_{jl,k} - g_{jk,l}), \tag{12}$$

where $(g^{il}) = (g_{il})^{-1}$ is the inverse matrix.

In the notation used here, the tensor matrix (11) entries are

$$g_{yy} = d_a^2/z^2 \quad \text{and} \quad g_{zz} = d_a^4/z^4 \tag{13}$$

and the inverse of the tensor matrix (11) entries are

$$g^{yy} = 1/g_{yy} = z^2/d_a^2 \quad \text{and} \quad g^{zz} = 1/g_{zz} = z^4/d_a^4. \tag{14}$$

Then, adapting this notation used for coordinates (y, z), non-zero expressions (12) are the following:

$$\Gamma^y_{yz} = \Gamma^y_{zy} = \frac{g_{yy,z}}{2g_{yy}} = -\frac{1}{z}, \tag{15}$$

$$\Gamma^z_{yz} = -\frac{g_{yy,z}}{2g_{zz}} = \frac{z}{d_a^2}, \tag{16}$$

and

$$\Gamma^z_{zz} = \frac{g_{zz,z}}{2g_{zz}} = -\frac{2}{z}. \tag{17}$$

To get the geodesic's differential equations, I first write them in standard notation,

$$\frac{d^2x^i}{dt^2} + \sum_j \sum_k \Gamma^i_{jk} \frac{dx^j}{dt} \frac{dx^k}{dt} = 0. \tag{18}$$

Then, adapting to the notation used in this paper, I obtain the differential equations for the geodesic $\gamma(t) = (y(t), z(t)$ as follows.

$$y'' - \frac{2}{z}y'z' = 0 \tag{19}$$

and

$$z'' + \frac{z}{d_a^2}y'^2 - \frac{2}{z}z'^2 = 0, \tag{20}$$

where the 'prime' means '$\frac{d}{dt}$'.

7.1 y-geodesics and z-geodesics

A y-geodesic starting at (y_1, z_1) in the direction of vector ∂_y has the equation $\gamma(t) = (y(t), z_1)$, where $y(t) = B_1 t + y_1$ is given by (19) with $z' = 0$. To get B_1, I set the conditions for the geodesic unit speed, $||\gamma'(t)|| = 1$,

$$||\gamma'(t)|| = \sqrt{g_{yy}y'^2(t)} = \sqrt{\frac{d_a^2}{z_1^2}B_1^2} = 1, \tag{21}$$

and hence, $B_1 = z_1/d_a$. Thus, $y(t) = (z_1/d_a)t + y_1$ where t is the arc-length. In fact, taking $y(t_2) = y_2$ and solving it for t_2 we easily obtain the distance

$$d(y_1, y_2) = t_2 = \frac{d_a}{z_1}(y_2 - y_1), \tag{22}$$

which agrees with (8).

A z-geodesic starting at (y_1, z_1) in the direction of the vector ∂_z has the equation $\gamma(t) = (y_1, z(t))$, so that $y' = 0$. Using it in (20), I obtain $z''/z' = 2z'/z$ to get $\ln z' = 2\ln z + \ln C_1$ and hence, $z' = C_1 z^2$. This last equation is easily solved for the initial condition to obtain

$$z(t) = -\frac{1}{C_1 t - 1/z_1}. \tag{23}$$

To get C_1, I differentiate (23) and write the unit speed condition $\sqrt{g_{zz}z'^2(t)} = 1$ to derive the unit-speed z-geodesic,

$$z(t) = -\frac{1}{t/d_a^2 - 1/z_1}. \tag{24}$$

Again, solving $z(t_2) = z_2$ for t_2, I derive the distance

$$d(z_1, z_2) = t_2 = d_a^2\frac{z_2 - z_1}{z_1 z_2}. \tag{25}$$

The last result confirms the fact that visual space is bounded by the horizon. The total length to the horizon from the point $(0, z_0)$, the closest point that can be fixated binocularly, is

$$d(z_0, \infty) = \lim_{z_2 \to \infty} d_a^2\frac{1 - z_0/z_2}{z_0} = \frac{d_a^2}{z_0}, \tag{26}$$

meaning that the z-geodesic is incomplete.

Further, the distance from $(0, z_0)$ to the eyes' resting posture fixation is $d(z_0, d_a) = d_a^2/z_0 - d_a$, which means that the distance from the horopter to the horizon is d_a.

The geodesics can be obtained starting at (y_1, z_1) in an arbitrary direction by solving first (19) for y' in terms of z and substituting it into (20), which can then be transformed into the Ermakov equation. Its solution is given in [18].

8 The Riemannian Curvature

Here the derivation of the Riemannian curvature of visual space is only sketched for the eyes' resting vergence posture and a more complete introduction to this complex object will be given elsewhere. In the basis vectors ∂_i, where the index runs here over y and z, the covariant differentiation ∇_{∂_i} on the basis vectors is

$$\nabla_{\partial_j}\partial_k = \sum_m \Gamma^m_{jk}\partial_m, \tag{27}$$

Following [14], the index notation of the curvature tensor can be written as,

$$\sum_m R^m_{jkl}\partial_m = \nabla_{\partial_j}\nabla_{\partial_l}\partial_k - \nabla_{\partial_l}\nabla_{\partial_k}\partial_j, \tag{28}$$

which, in low indices, is the following:

$$R_{ijkl} = \sum_m g_{im}R^m_{jkl}. \tag{29}$$

Using the notation corresponding to coordinates (y, z): (13); (15); (16); (17) and (27), the Riemannian curvature tensor can be calculated as follows,

$$\begin{aligned} R_{yzyz} &= -\frac{1}{2}g_{yy,zz} + \frac{g^2_{yy,z}}{4g_{yy}} + \frac{g_{yy,z}g_{zz,z}}{4g_{zz}} \\ &= -\frac{3d_a^2}{z^4} + \frac{d_a^2}{z^4} + \frac{2d_a^2}{z^4} = 0. \end{aligned} \tag{30}$$

Thus, in this case of the eyes' resting vergence posture, the curvature tensor of visual space vanishes identically and visual space is flat for this particular eye fixation [14].

9 Numerical Results and A Comparison with Other Studies

We note first, as the simulations clearly show, that visual space geometry is shaped by physical space being expanded between the head and the frontal line horopter at the abathic distance d_a and compressed beyond the horopter. These changes in perceived depth when the eyes are in their resting vergence posture (corresponding to the eye's lens tilt's angle β) make the geodesics incomplete such that visual space is bounded by the horizon in the direction of the gaze.

For the numerical calculations, I assume the human average lens tilt $\beta = 3.3°$, which gives the average abathic distance $d_a = 99.61$ cm [22]. I also estimate that $z_0 = 3$ cm. Using these values in the geodesic distance expressions, I obtain the total distance to the horizon,

$$d(z_0, \infty) = \frac{d_a^2}{z_0} = \frac{0.9961^2}{0.03} \approx 33 \text{ m}, \tag{31}$$

and the distance to the horopter at the abathic distance fixation,

$$d(z_0, d_a) = \frac{d_a^2}{z_0} - d_a \approx 32 \text{ m}. \tag{32}$$

Therefore, the distance from the horopter at the abathic distance to the horizon is $d(d_a, \infty) \approx 1$ m.

The finite distance to the horizon should be expected as we perceive objects in the horizontal binocular field against the horizon with the depth perception resulting from the metric (9) such that our field of vision appears two-dimensional with the objects initially located in visual processing at different distances from the horopter and finally perceived against the egocentric coordinates.

In literature, the distance of the vanishing points at the horizon is reported to be between 6 m and 100 m, see [8]. Here, the AE model in the binocular system determines the eyes' resting vergence posture abathic distance that depends

on the lens tilt angle β. The simulations were carried out for three values of the abathic distances; $d_a(0.5°) = 40.2$ cm, $d_a(3.3°) = 99.61$. cm, and $d_a(4°) = 157.75$ cm. For these values, I obtain the distance to the horizon 5.4 m, 33 m, and 83 m, respectively. Thus, the geometric theory of the binocular perception developed in [22] and extended here to iso-disparity curves, unifies in one theory the distances to the horizon reported in the literature, where precise explanations for the differences in these distances were not provided.

The curvature of visual space, derived here for the eyes' resting vergence posture when they fixate at the abathic distance, is zero, so the visual space is flat for this particular eyes posture. In this case, the iso-disparity curves are frontal line geodesics that are parallel to the y-axis and the z-geodesics are straight lines perpendicular to the y-geodesics. The z-geodesics are incomplete and their total lengths determine the distances to the horizon in the gaze direction.

For all other fixations, see the iso-disparity conics representing the two families of visual geodesics in Figure 4 and Figure 5: for short-distance fixations the geodesics are ellipses, while for far-distance fixations the geodesics are hyperbolas. For the precise classification of the horopter's shape and, hence, the iso-disparity curves' shape with respect to the fixation point in the binocular field, see [22].

Because the geodesics are converging in the case of the elliptic iso-disparity family, the curvature of visual space is positive. Similarly, because the geodesics are diverging in the case of the hyperbolic iso-disparity family, the curvature of visual space is negative. The numerical value cannot be readily obtained in both cases as the problem of getting the metric from unparametrized geodesics is still open in Riemannian geometry [5].

The results obtained here, although not complete, revise the abstract geometric theories of binocular phenomenal space, most notably, a constant negative-curvature hyperbolic geometry of visual space originally proposed by Luneburg [15] in the 1940s and further developed in [4] and [11], among other publications.

Luneburg's approach is one of three theories that used axiom-based model geometries (Euclidean, hyperbolic, and spherical) to model phenomenal spatial relations. These approaches, however, were not supported by experimental data and did not pay attention to biological and psychological aspects of human vision. For example, Luneburg's theory uses the Vieth-Müller circle (VMC) as the geometric horopter. In [20], I showed that the VMC is anatomically inaccurate as a geometric horopter. In fact, it incorrectly assumes the nodal point located at the eye's rotation center [10], which provides a good numerical approximation of the geometric horopter close to the fixation point. More significantly, when the VMC is compared with the simulated horopteric hyperbolas in [22], their difference in periphery is very large. Thus, the modeling based on the VMC will significantly distort the ambient space geometry provided by the coarse disparity, see the discussion in Section 5.

Beyond these three theories, there are also theories based on Riemann's approach to studying abstract space with defined metric function. One of the most general distance-defined spaces is called metric space. These theories model visual space's measurable properties such as distances and angles while also including stimulus location in physical space and psychological factors [24]. The theory proposed here for modeling visual space spatial relations is similar to the metric-based theories but also includes anatomical and physiological aspects of the human visual system.

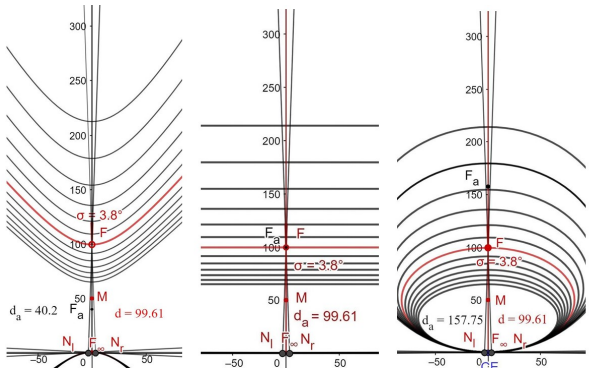

Figure 8: Three simulations for the same fixation and different values of the AE's lens' tilt. On the left, the lens' tilt $\beta = 0.5°$, in the middle, $\beta = 3, 3°$, and on the right, $\beta = 4°$. In these cases, the curvature is negative, zero and positive, resoectively.

Of the many other studies reporting results on phenomenal geometry, the experimentally obtained values of the visual space's curvature in [13] are closest to the results obtained in the presented here studies. However, the geometric theory of of disparity-based perception developed here, refines the experimental results in [13].

It is demonstrated in the simulations shown in Figure 8. [13] found that the curvature changes from elliptic in near space to hyperbolic in far space. For very large distances, the visual plane became parabolic. Figure 8, in addition, shows that the curvature of visual space depends on the AE model parameters for the same symmetrically fixated point at the distance $d = 99.61$ cm. In the left panel of Figure 8, the iso-disparity curves are hyperbolas for the lens's tilt $\beta = 4°$, while in the middle panel the iso-disparity curves are straight frontal lines for the lens' tilt $\beta = 3.3°$ and, on the right, they are ellipses for the lens' tilt $0.5°$.

10 Conclusions

In this preliminary study, I examined the Riemannian geometry framework in modeling global aspects of spatial relations in phenomenal visual space based on simulated iso-disparity curves. The numerical results derived here are based on the postulated relative depth relation (7). This relation will be thoroughly re-examined based on the fundamental issues underlying the human vision system articulated in Section 4.

The most important results obtained in this work include the curvature of visual space which depends on the binocular fixation point's location in the horizontal visual plane and the eyes' asymmetry parameters: the fovea's displacement from the posterior pole and the crystalline lens' tilt. The curvature is zero for the eyes' resting vergence posture at the abathic distance fixation that is distinguished by the family of frontal iso-disparity lines [22]. For other eye postures, which are classified in terms of the fixation point in the visual plane [22], the visual space curvature has a nonzero value. In these cases, the simulated elliptic iso-disparity curves' convergence and hyperbolic iso-disparity curves' divergence indicate the positive curvature and negative curvature of visual space, respectively.

Although metric cannot be readily obtained for unparametrised geodesics [5], the convergence of the elliptic iso-disparity conics and the divergence of the hyperbolic iso-disparity conics can, in principle, allow for a study of the rates of convergence/divergence based on my *GeoGebra* simulations (recall Figure 4 and Figure 5). These rates can help to estimate the Gaussian curvature's numerical values for each of the binocular fixations.

Acknowledgements

I thank Alice Turski for her editing this manuscript.

References

[1] P. Artal, Optics of the eyes and its impact in vision, Adv. Opt. Photon, 6, 340-367 (2014).

[2] S.R. Barry, Beyond the critical period. Acquiring stereopsis in adulthood. In Plasticity in Sensory Systems. Steeves J.K. and Harris L.R. (eds.). Cambridge University Press. 175-195 (2013).

[3] C. Blakemore, The Range and Scope of Binocular Depth Discrimination in Man. J. Physiol. 211, 599-622 (1970).

[4] A.A. Blank, The Luneburg theory of binocular visual space, J. Opt. Soc. Am., 43, 717-727 (1953).

[5] K. Burns, V.S. Matveev, Open problems and questions about geodesics, Ergodic Theory and Dynamical Systems, 41, 641-684 (2021).

[6] M.P. Do Carmo, Riemannian Geometry, Birkhäuser, Boston, 1993.

[7] S.M. Ebenholtz, Oculomotor Systems and Perception, Cambridge U Press, 2001.

[8] C.J. Erkelens, Perspective space as a model for distance and size perception, i-Perception, 1-20 (2017).

[9] D. Guitton, M. Volle, Gaze control in humans: eye-head coordination during orienting movements to targets within and beyond the oculomotor range, J. Neurophysiol., 58, 427-459 (1987).

[10] W.L. Gulick and R.B. Lawson, Human stereopsis: A psychophysical analysis. New York: Oxford University Press 1976.

[11] T. Indow, A critical review of Luneburg's Model with regard to global structure of visual space, Psychological Review, 98, 430-453 (1991).

[12] W. Jaschinski-Kruza, Eyestrain in VDU users: viewing distance and the resting position of ocular muscles, Hum. Factors, 33, 69-83 (1991).

[13] J.J. Koenderink, A.J. van Doom, J. S. Lappin, Direct measurement of the curvature of visual space, Perception, 29, 69-79 (2000).

[14] J.M. Lee, Riemannian Manifolds: An Introducton to Curvature, Springer. 1997.

[15] R.K. Luneburg, Mathematical Analysis of Binocular Vision, Princeton University Press, 1947.

[16] G. Maiello, M. Chessa, P.J. Bex, F. Solari, Near optimal combination of disparity across a log-polar scaled visual field, PLoS Comp. Biol., 16(4):e1007699 (2020).

[17] A.M. Norcia, E.E. Sutter, C.W. Tyler, Electrophysiological evidence for the existence of coarse and fine disparity mechanisms in human, Vis. Res., 25, 1603-1611 (1985).

[18] A.D. Polyanin, V.F. Zaitsev, Handbook of Exact Solutions for Oridinary Differential Equations, CRC Press LLC, Boca Raton, 2003.

[19] T. Shipley and S. Rawlings, The Nonius Horopter–II. An Experimental Report, Vis. Res., 10, 1263-1299 (1970).

[20] J. Turski, On binocular vision: the geometric horopter and cyclopean eye, Vis. Res., 119, 73–81 (2016).

[21] J. Turski, Binocular system with asymmetric eyes, J. Opt. Soc. Am. A 35, 1180-1191 (2018).

[22] J. Turski, A geometric theory integrating human binocular vision with eye movement, Front. Neurosci. 14:555965, 1-17 (2020).

[23] G. von Noorden and E.C. Campos, Binocular Vision and Ocular Motility: Theory and Management of Strabismus. Mosby, A Harcourt Health Sciences Company, St. Louis, 1974.

[24] M. Wagner, The Geometries of Visual Space, Lawrence Erlbaum Associates, Mahwah, NJ, 2006.

[25] L.M. Wilcox and R.S. Allison, Coarse-fine dichotomies in human stereopsis. Vis. Res. 49,2653-2665 (2009).